Dalton Transactions

Electrochemical Reduction of CO_2 to CO and $HCOO^-$ on Metal-Cyclam Complex Catalysts: Selectivity and Limiting Potential from DFT

Journal:	*Dalton Transactions*
Manuscript ID	DT-ART-06-2021-002159
Article Type:	Paper
Date Submitted by the Author:	29-Jun-2021
Complete List of Authors:	Masood, Zaheer; Southern Illinois University, Department of Chemistry and Biochemistry Ge, Qingfeng; Southern Illinois University, Department of Chemistry and Biochemistry

Electrochemical Reduction of CO_2 to CO and $HCOO^-$ on Metal-Cyclam Complex Catalysts: Selectivity and Limiting Potential from DFT

*Zaheer Masood and Qingfeng Ge**

Department of Chemistry and Biochemistry, Southern Illinois University, Carbondale, IL 62901, USA.

AUTHOR INFORMATION

Corresponding Author: Qingfeng Ge, Department of Chemistry and Biochemistry, Southern Illinois University, Carbondale, IL 62901, United States. orcid.org/0000-0001-6026-6693. Email: qge@chem.siu.edu.

Author: Zaheer Masood, Department of Chemistry and Biochemistry, Southern Illinois University, Carbondale, IL 62901, United States. orcid.org/0000-0003-2836-3754

Abstract

Sustainable fuel production from CO_2 through electrocatalytic reduction is promising but challenging due to high overpotential and poor product selectivity. Herein, we computed the reaction free energies of electrocatalytic CO_2 reduction to CO and $HCOO^-$ using the density functional theory method and screened the transition metal(M) - cyclam(L) complexes as molecular catalysts for CO_2 reduction. Our results showed that pK_a of the proton adduct formed from protonation of the reduced metal center can be used as a descriptor to select operating pH of the solution to steer the reaction toward either the CO or hydride cycle. Among the complexes, $[LNi]^{2+}$ and $[LPd]^{2+}$ catalyze the reactions following the CO cycle and are the CO selective catalysts in the pH ranges of 1.81 - 7.31 and 6.10 and higher, respectively. Among the complexes that catalyze the reactions following the hydride cycle, $[LMo]^{2+}$ and $[LW]^{3+}$ are the $HCOO^-$ selective catalysts and have low limiting potentials of -1.33 V and -1.54 V, respectively. Other complexes, including $[LRh]^{2+}$, $[LIr]^{2+}$, $[LW]^{2+}$, $[LCo]^{2+}$, and $[LTc]^{2+}$ will catalyze the reactions resulting in either $HCOO^-$ from CO_2 reduction or H_2 from proton reduction while $HCOO^-$ formation is always thermodynamically more favorable. Notably, $[LMo]^{2+}$, $[LW]^{3+}$, $[LW]^{2+}$ and $[LCo]^{2+}$ have a limiting potential less negative than -1.6 V and are based on earth-abundant elements, making them attractive for practical application.

I. Introduction

Conversion of CO_2 to value-added chemicals and fuel using renewable energy-based technology would help alleviate our dependence on fossil fuels and mitigate the rising concentration of CO_2 in the atmosphere[1-3]. The electrochemical reduction of CO_2 is a promising approach as the reaction can be interfaced with renewably generated electricity under mild conditions. However, implementing the electrochemical reduction of CO_2 is challenging as highly efficient and selective catalysts with a low overpotential are needed but not yet available.

Electrochemical CO_2 reduction can be catalyzed with a solid catalyst in a heterogeneous system[4, 5] or a molecular catalyst in a homogeneous system[6, 7]. Molecular catalysts have the advantage of optimizing performance through the tuning of active centers at the atomic level. Both metal centers[8, 9] and ligands[10-12] in a molecular catalyst can be systematically changed to optimize catalytic activity and selectivity. CO and $HCOO^-$ are the major products of CO_2 electrocatalytic reduction with molecular catalysts. It has been observed that porphyrin[13-16] and phthalocyanine[17, 18] with Fe and Co as metal centers are selective to CO, whereas those with Rh, In, and Sn are selective to $HCOO^-$ [8, 14]. Other catalysts, P_2N_2 (P_2N_2 = 1,5-diaza-3,7-diphosphacyclooctane) with Rh[19], pincer complexes with Ir[20], $[Pt(dmpe)_2]^{2+}$ [21, 22], iron carbonyl cluster[23, 24], $[Ni(dmpe)2]^{2+}$ [25] and $[Pd(depe)_2]^{2+}$ [26] have shown $HCOO^-$ selectivity.

Density functional theory (DFT) studies have been widely used to provide mechanistic insights into electrocatalytic reduction of CO_2. In heterogeneous electrocatalysis, descriptors have been developed to screen and select catalysts with high efficiency and selectivity for CO_2 reduction [27-30]. Descriptor-based studies on electrochemical CO_2 reduction on molecular catalysts are rare[21, 31]. Ceballos and Yang introduced hydricity of metal-hydride complex as a descriptor for $HCOO^-$ selectivity[21]. Based on the correlation between standard redox potentials and pK_as for the aromatic nitrogen-heterocycles molecules, Marjolin and Keith proposed to use the computationally derived

Pourbaix diagram triple points to predict catalysts that would facilitate proton and electron transfers for efficient CO_2 reduction[31]. On the other hand, most studies on molecular catalysts focus on using the potential energy profile along the reaction pathway from computationally optimized reactant, intermediate and product structures to predict the limiting potential, proton-coupled electron transfer (PCET)[32, 33] steps and product selectivity.

Cyclam, i.e., 1,4,8,11-tetraazacyclotetradecane, is a class of water-soluble macrocycle ligands, which binds strongly to many metal ions[34-36]. Ni-cyclam has been tested as a catalyst for the electrochemical reduction of CO_2 and exhibits promising reactivity and CO-selectivity[37-41]. Mechanistic studies establish that CO_2 is activated by forming η^1-CO_2 adduct on the reduced metal center of Ni-cyclam and then reduced to CO through concerted proton-electron transfer steps[33, 42]. Can other metal-cyclam complexes act as electrocatalysts to reduce CO_2? If they are, will they be only selective toward CO? With these questions in mind, we investigated metal-cyclam complexes, $[(cyclam)M]^n$ (Figure 1[43], trans-III isomer) or $[LM]^n$, with various transition metal ions (M = Cr, Mn, Fe, Co, Ni, Mo, Tc, Ru, Rh, Pd, W, Re, Os, Ir, and Pt) for electrocatalytic CO_2 reduction based on reaction free energies determined from DFT calculations. We show that pKa of the proton adduct can be utilized as a descriptor to identify a metal center on which the reduction follows either the CO or hydride cycle. For the catalysts that facilitate the hydride cycle, we developed a quantitative relationship between the first reduction potential of catalysts and BDFE of the M-H bond, which can be used as a measure of the formation free energy of $HCOO^-$. The results allowed us to identify the CO selective catalysts and determine the operating pHs as well as the $HCOO^-$ selective catalysts based on earth-abundant metals.

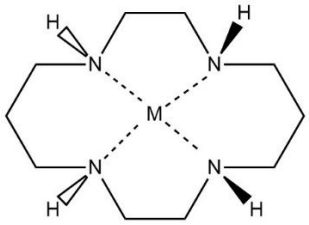

Figure 1. Trans III cyclam conformation with a metal center, M (M = Cr, Mn, Fe, Co, Ni, Mo, Tc, Ru, Rh, Pd, W, Re, Os, Ir, and Pt with different oxidation states).

II. Results and Discussion

To validate the methodology and adequacy of theory level and basis sets, we compared our calculated reduction potential of $[LNi]^{2+}$ (Ni-cyclam) with both previous experimental[37] and computational studies[33]. The experimental study reported a reduction potential of -0.90 V for $[LNi]^{2+}$ in an aqueous solution at pH 4.1, corresponding to a standard reduction potential of -0.66 V. Our calculated standard reduction potential is -0.64 V, in very good agreement with the experimental result. We note that Song et al.[33] reported a reduction potential of -1.12 V for $[LNi]^{2+}$. A closer examination revealed that our calculated reaction free energy for the reduction from $[LNi]^{2+}$ to $[LNi]^{+}$ differ from their value by only 3.18 kJ/mol (equivalent to ~ 0.03 V in reduction potential). Considering the differences in the code, basis sets and functionals used in these studies, the level of agreement is quite remarkable. The difference in the calculated standard reduction potential can be attributed to the different solvent models used in the studies: we used an implicit aqueous solvent model whereas Song et al. used a solvation model simulating a 1:4 mixture of water and acetonitrile. The calculated reduction potentials of $[LMo]^{2+}$ (4d metal) and $[LW]^{3+}$ (5d metal) using B3LYP-D3 were compared with those based on MN15, a hybrid meta-GGA functional, which is considered to be more accurate for 4d and 5d metals[44]. The calculated

reduction potentials of $[LMo]^{2+}$ and $[LW]^{3+}$ with MN15, -1.23 V and -1.46 V, respectively, are in reasonably good agreement with -1.33 V and -1.54 V, respectively, from B3LYP-D3.

We examined metal ions of elements in groups 6 to 10 and series 3d to 5d coordinated with the cyclam macrocycle. For groups 6 to 8, the metal ions may exist at different oxidation states. In fact, different oxidation states for these elements were reported in previous studies, e.g. Co (II)[45], Co (III)[46], Cr (II)[47] and Cr (III)[48]. We calculated the first reduction potential (E°) for complexes with the metal ion in 3+, 2+ and 1+ initial oxidation state for groups 6 to 9 and used E° as a criterion to select the potential catalyst for CO_2 reduction. The reduction potentials for CO_2/CO and CO_2/HCOOH are -0.104 V[49] and -0.199 V[49, 50] (vs. SHE), respectively. Therefore, metal-cyclam complexes with E° more positive than -0.104 V were ruled out as CO_2 reduction catalysts since they cannot reduce CO_2 to either CO or $HCOO^-$. Calculated first reduction potentials for metal ions of Cr, Mn, Fe, Co, Ru, Rh, Os and Ir in the 3+ oxidation states of the complexes have been presented in Table S1 in Supporting Information. Based on the above criterion, the 3+ oxidation state of these complexes was excluded from further studies. For group 10, only the 2+ oxidation state was considered.

Electrocatalytic CO_2 reduction to $HCOO^-$ [51] and CO[49] in an aqueous medium may occur according to the following reactions:

$$CO_{2(g)} + H^+_{(aq.)} + 2e^- \longrightarrow HCOO^-_{(aq.)} \qquad (1)$$

$$CO_{2(g)} + 2H^+_{(aq.)} + 2e^- \longrightarrow CO_{(g)} + H_2O_{(l)} \qquad (2)$$

Figure 2 shows the origin of selectivity of either hydride or CO during CO_2 electrochemical reduction. The electrocatalytic reduction of CO_2 starts with the formation of the nucleophile ($[LM]^{(n-1)}$) by reducing the parent electrocatalyst[52-54] (step i). $[LM]^{(n-1)}$ can then react either with a proton, branching out to the hydride cycle (step ii), or with CO (step iii), bifurcating to the CO

cycle[55]. The reaction free energy of the protonation step ($\Delta G_{rxn}(PT)$) (eqn. 3) determines whether the formation of the proton adduct ($[LM\text{-}H]^{(n)}$) is favorable or not:

$$[LM]^{(n-1)} + H^{+} \longrightarrow [LM\text{-}H]^{n} : \Delta G_{rxn}(PT) \qquad (3)$$

where $\Delta G_{rxn}(PT)$ relates to pK_a of $[LM\text{-}H]^{n}$ and pH through eqn. 4.

$$\Delta G_{rxn}(PT) = 2.303RT(pH - pK_a[LM\text{-}H]^{n}) \qquad (4)$$

Therefore, $\Delta G_{rxn}(PT)$ (step ii) can be tuned by adjusting pH relative to the pK_a of $[LM\text{-}H]^{n}$. If pH is set at a value lower than the pK_a of $[LM\text{-}H]^{n}$, $\Delta G_{rxn}(PT)$ is negative, indicating that protonation is exergonic, which will drive the reaction into the hydride cycle. In contrast, if pH > pK_a, protonation will not be thermodynamically favorable. In the latter case, the metal ion will be open for CO_2 binding and steer the reaction to the CO cycle through step iii.

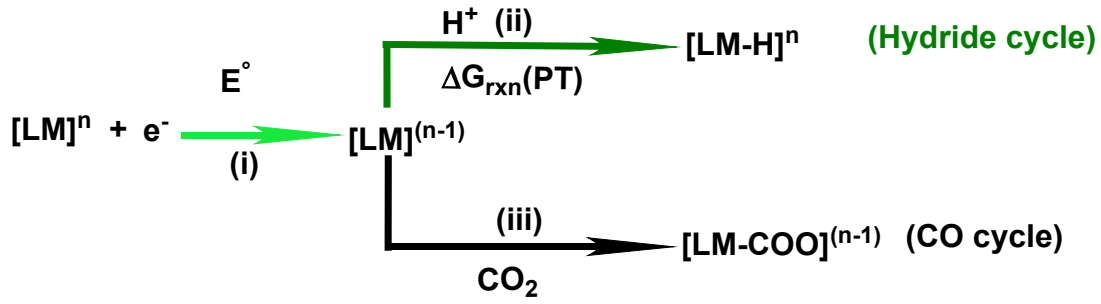

Figure 2. The first two steps in electrocatalytic pathways of CO_2 reduction leading to hydride and CO cycle in an aqueous medium on the cyclam based catalyst (L =cyclam and M = metal center). The light green arrow shows common step shared by the hydride and CO cycles, Numbers in parenthesis show step number.

The hydride and CO cycle bifurcate from $[LM]^{(n-1)}$ and the reaction can proceed through either the hydride or CO cycle, depending on the pK_a of $[LM\text{-}H]^{n}$. Figure 3 presents the computed pK_a values of $[LM\text{-}H]^{n}$ for all complexes with different metal centers at 3+, 2+ and 1+ oxidation states. The pK_a values of the metal-cyclam complexes for the metal ions at the same oxidation

state decrease in general from left to right across the periodic table, whereas the pK_a value of $[LM\text{-}H]^{+}$ is higher than those of $[LM\text{-}H]^{2+}$ and $[LM\text{-}H]^{3+}$.

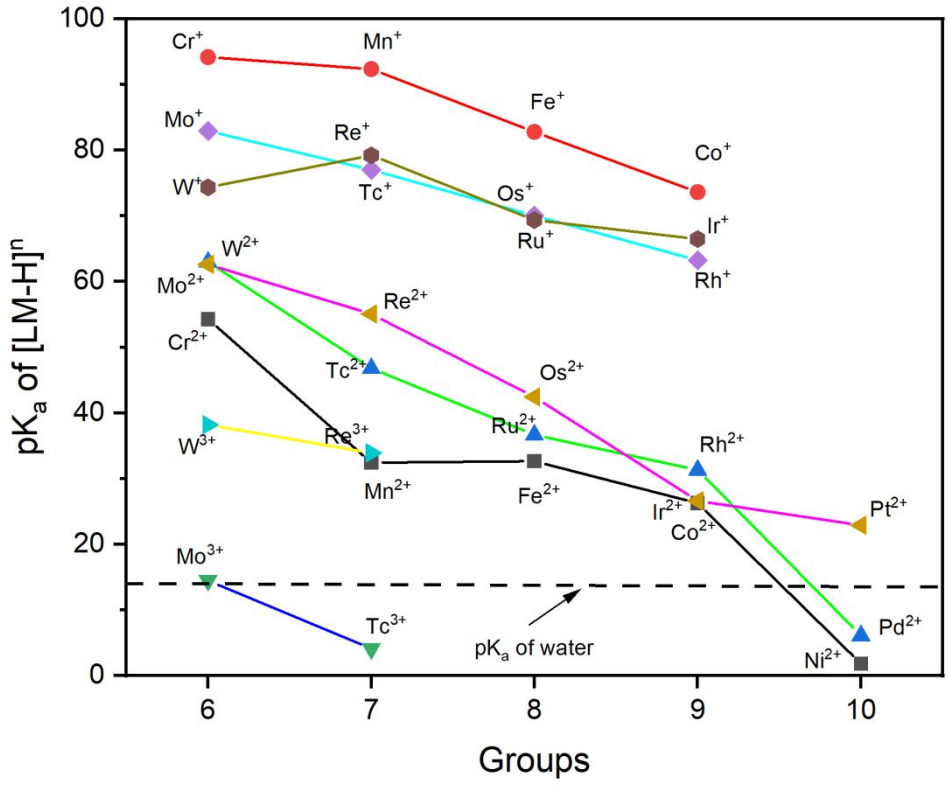

Figure 3. The computed pK_a values of $[LM\text{-}H]^{n}$ for metal ions in cyclam used in this study (The solid lines are guide for the eye).

Overall, decreasing pK_a value corresponds to a decrease in Brønsted acidity from left to right across the periodic table and from top to bottom in a group. Figure 3 also shows that most $[LM\text{-}H]^{n}$ have pK_a values higher than 14 (pK_a of water) except for $[LNi\text{-}H]^{2+}$, $[LPd\text{-}H]^{2+}$ and $[LTc\text{-}H]^{3+}$. Based on eqn. 4, $\Delta G_{rxn}(PT)$ will always be negative for the metal-cyclam complexes with $pK_a > 14$ even under the most basic conditions. On the other hand, $\Delta G_{rxn}(PT)$ can be positive or negative for the complexes with $pK_a < 14$, depending on pH. The metal-cyclam complexes with

pK_a > 14 will always drive the reaction to follow the hydride cycle, whereas $[LNi]^+$, $[LPd]^+$ and $[LTc]^{3+}$ have the potential to catalyze the CO cycle by controlling pH > pK_a of $[LM\text{-}H]^n$. Therefore, $[LNi]^+$, $[LPd]^+$ and $[LTc]^{3+}$ will first bind CO_2 and then facilitate the reactions to follow the CO cycle. In the following, we will discuss these CO selective catalysts first.

The CO Cycle. The experimental pK_a value of 1.81[56] for $[LNi\text{-}H]^{2+}$ was used as a reference for the determination of pK_a values of other complexes within the isodesmic proton exchange scheme, as detailed in section 1 of Supporting Information. Accordingly, pK_a of 6.10 and 4.10 for $[LPd\text{-}H]^{2+}$ and $[LTc\text{-}H]^{3+}$, respectively, were obtained. Based on eqn. 4, protonation of $[LNi]^+$, $[LPd]^+$ and $[LTc]^{2+}$ will not be spontaneous if the pH of the reaction solution is held at a value higher than the corresponding pK_a. Under such a condition, CO_2 can bind $[LNi]^+$, $[LPd]^+$ and $[LTc]^{2+}$ to form $[LNi\text{-}COO]^+$, $[LPd\text{-}COO]^+$ and $[LTc\text{-}COO]^{2+}$ adducts, respectively, and eventually be reduced to CO after completing the CO cycle (Figure 5). To facilitate CO_2 binding, the formation of the CO_2 adduct with $[LNi]^+$, $[LPd]^+$ and $[LTc]^{2+}$ needs to be more competitive energetically than the protonation of the metal ion of those complexes. Protonation free energies of $[LNi]^+$, $[LPd]^+$ and $[LTc]^{2+}$ were calculated to be -10.25, -34.77 and -23.38 kJ/mol, respectively, at pH = 0. The free energy of $CO_{2(g)}$ binding at 1 atm $CO_{2(g)}$ on these metal ions in the complex are 5.77, 18.49 and 48.39 kJ/mol, respectively (eqn.5).

$$[LM]^+ + CO_{2(g)} \longrightarrow [LM\text{-}COO]^+ : \Delta G^{\circ}_{rxn}[LM\text{-}COO]^+_{(CO2(g))} \qquad (5)$$

According to eqn. 4, the free energy of protonation equals to the free energies of $CO_{2(g)}$ binding (eqn. 5) at pH = 2.82 for $[LNi]^+$, pH = 9.34 for $[LPd]^+$ and pH =12.60 for $[LTc]^{2+}$. Under acidic pH, CO_2 may participate in the reaction as H_2CO_3,

$$[LM]^+ + H_2CO_{3(aq.)} \longrightarrow [LM\text{-}COO]^+ + H_2O_{(l)} \quad : \Delta G^{\circ}_{rxn}[LM\text{-}COO]^+_{(H2CO3)} \qquad (6)$$

The formation energies of the CO_2 adducts from H_2CO_3, based on the reaction shown in eqn. 6 are -24.24 , -11.52 and 18.38 kJ/mol for $[LNi]^+$, $[LPd]^+$ and $[LTc]^{2+}$ respectively. The significantly lower $\Delta G^{\circ}_{rxn}[LM\text{-}COO]^+_{(H2CO3)}$ indicates that the dissolved CO_2 in the form of H_2CO_3 in an aqueous solution will make the formation of CO_2 adducts exergonic for $[LNi]^+$ and $[LPd]^+$ but not on $[LTc]^{2+}$ under the acidic pH of electrochemical reduction of CO_2. Furthermore, the protonation free energy of $[LTc\text{-}COO]^{2+}$ (defined in eqn. 4) is positive even at pH = 0 (13.30 kJ/mol) as pK_a of $[LTc\text{-}COOH]^{3+}$ is 2.33, making $[LTc]^{3+}$ not a catalyst for CO_2 reduction to CO. Therefore, we excluded $[LTc]^{3+}$ from further study.

Generally, CO_2 binds the metal centers in the η-CO_2 coordination in the $[LM\text{-}COO]^+$ complexes formed with $[LNi]^+$ and $[LPd]^+$ [57]. The optimized molecular geometries (top and side view) of the $[LM\text{-}COO]^+$ complexes together with the HOMO and LUMO molecular orbitals are summarized in Figure 4. The upper row of Figure 4 collects the optimized geometries of $[LNi\text{-}COO]^+$ in top and side views, the LUMOs and HOMOs of $[LNi\text{-}COO]^+$, $[LNi]^+$ and CO_2 and lower rows are for the $[LPd]^+$ complexes. The interaction between CO_2 and the metal center is primarily through the stabilized LUMOs ($2\pi_g$) of CO_2 and β-HOMOs (predominantly dz^2 of the metal) of the metal complexes. In addition, CO_2 bound to $[LNi]^+$ is further stabilized by the hydrogen bonding through both oxygen atoms of CO_2 to the H atoms of the ligand. The O-C-O bond angle is 139.07˚, consistent with the fact that CO_2 is in an activated configuration. On the other hand, only one oxygen atom of $[LPd\text{-}COO]^+$ is close enough to facilitate hydrogen bonding interaction due to a longer Pd-C bond length (2.11 Å) than Ni-C (2.08 Å), resulting in a weaker binding of CO_2 to $[LPd]^+$. The O-C-O bond angle of $[LPd\text{-}COO]^+$ is 139.64˚, consistent with the fact that CO_2 is

activated but to a lesser degree. The optimized $[LNi\text{-}COO]^+$ structure, including bond distances, O-C-O angle, as well as the general features of HOMO and LUMO, is in close agreement with the previous report[33]. We note that the stabilization of adsorbed CO_2 through hydrogen bonding has a significant contribution to the overall stabilization of adducts. To understand CO_2 binding in these complexes, we conducted AIM charge analysis of $[LM\text{-}COO]^+$ and presented the results in Table S2 of Supporting Information. The results of AIM analysis show that the net charge on CO_2 is ~ 0.1 |e| more negative in $[LNi\text{-}COO]^+$ (-0.66 |e|) than in $[LPd\text{-}COO]^+$ (-0.55 |e|). The AIM charges are consistent with the observation that CO_2 is in a more activated state in $[LNi\text{-}COO]^+$ than $[LPd\text{-}COO]^+$. These results show that direct $LUMO_{CO2}$ $HOMO_{[LM]+}$ interactions, hydrogen bonding with the ligand as well as charge transfer from the metal center to CO_2 contribute to the binding and activation of CO_2.

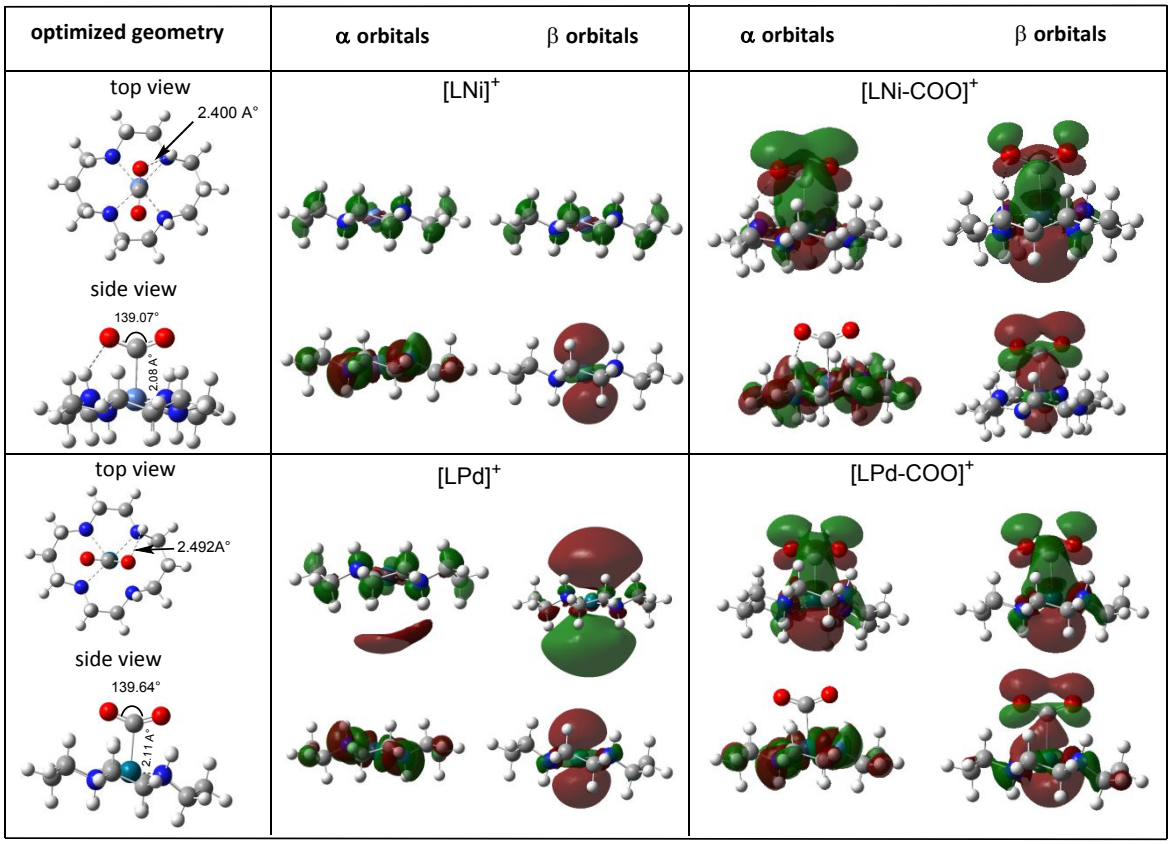

Figure 4. Upper rows: optimized molecular structure of $[LNi\text{-}COO]^+$(side view and top view), HOMOs and LUMOs of $[LNi]^+$ and $[LNi\text{-}COO]^+$. Lower rows: optimized molecular structure of $[LPd\text{-}COO]^+$(side view and top view), HOMOs and LUMOs of $[LPd]^+$, and $[LPd\text{-}COO]^+$.

Following the formation of CO_2 adducts, further reduction of CO_2 is completed through a series of electron and proton transfer steps, as shown in Figure 5 [33]. Reduction and protonation of $[LM\text{-}COO]^{(n-1)}$ leads to the carboxylate adduct ($[LM\text{-}COOH]^{(n-1)}$), which can be achieved through either concerted proton-electron transfer (CPET; $H+ + e^-$) (step iii) or sequential electron-proton transfer (SEPT; ET-PT) (step iv and v). The CPET process dominates at $pH \leq pK_a$ of $[LM\text{-}COOH]^{(n-1)}$. Combination of $[LM\text{-}COOH]^{(n-1)}$ with a proton causes $[LM\text{-}COOH]^{(n-1)}$ to dissociate into metal-carbonyl ($[LM\text{-}CO]^n$) (step vi) and water as a result of the C-O bond cleavage. Dissociation of $[LM\text{-}CO]^n$ to $[LM]^n$ and CO regenerates the catalyst (step vii). The reduction potentials of the initial catalysts E° and the CO_2 adducts (step iv) (vs. SHE), pK_a of $[LM\text{-}COOH]^+$, reaction free energy for proton transfer and the accompanied C-O bond cleavage as well as the dissociation energy of $[LM\text{-}CO]^n$ to CO and $[LM]^n$ for $[LNi]^{2+}$ and $[LPd]^{2+}$ are summarized in Table 1.

Table 1. The first reduction potential of $[LM]^{2+}$ (E°) and the reduction potential of CO_2 adducts (step iv) vs. SHE, pK_a values of $[LM\text{-}COOH]^+$, reaction free energy of proton transfer and C-O bond cleavage and dissociation energy of $[LM\text{-}CO]^{2+}$ to CO and $[LM]^{2+}$.

Catalyst	Red. Pot of $[LM]^n$ (V) (**i**)*	Red. Pot of $[LMCOO]^{(n-1)}$ (V) (iv)*	pK_a of $[LM\text{-}COOH]^+$	Proton transfer and C-O bond cleavage (kJ/mol) (vi)*	Dissociation energy of $[LM\text{-}CO]^n$ (kJ/mol) (vii)*
$[LNi]^{2+}$	-0.64	-0.95	7.31	-24.26	-10.77
$[LPd]^{2+}$	-1.21	-1.00	4.37	-120.04	-24.20

**Step number according to Figure 5*

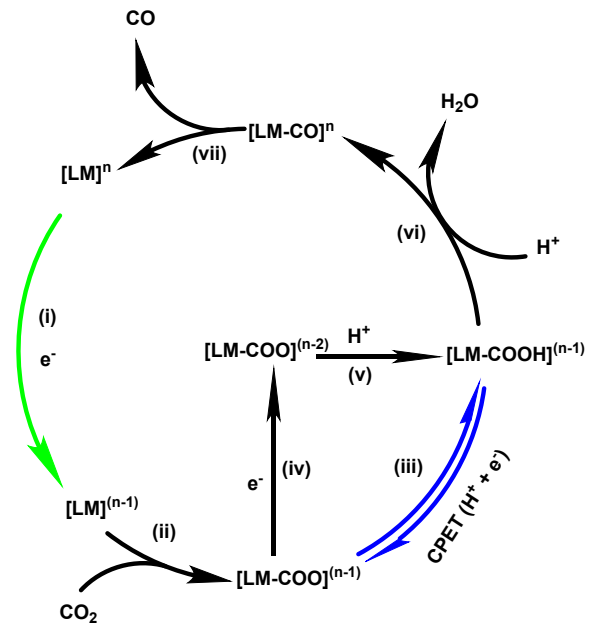

Figure 5. Electrocatalytic cycle of CO_2 reduction to CO. Bright green color arrow shows (step i) shared step with hydride cycle . Blue arrows show CPET step.

Ni(II) Cyclam Complex. The binding of CO_2 to $[LNi]^+$ to form $[LNi\text{-}COO]^+$ has already been discussed. The formation of $[LNi\text{-}COOH]^+$ from $[LNi\text{-}COO]^+$ can be achieved through either CPET (step iii) or SEPT (steps iv and v). The one-electron reduction potential of $[LNi\text{-}COO]^+$ following step iv was found to be -0.95 V. The calculated pK_a of $[LNi\text{-}COOH]^+$ is 7.31, corresponding to a neutral pH. In experimental studies, CO_2 reduction on $[LNi]^{2+}$ was carried out at pH 4.1 and 7.0. This pH range corresponds to a reduction potential range of -1.18 V and -1.37 V for step iv. The typically applied potential for CO_2 reduction is -1 ~ -1.3 V,[58-60] indicating that CO_2 reduction is less likely to proceed through SEPT under the experimental conditions. The pK_a of 7.31 for $[LNi\text{-}COOH]^+$ shows that CPET will be the dominant path at acidic or neutral pHs. At pH > 7.31, SEPT becomes the only possible mechanism, which will not be operable due to the more negative reduction potential than that for step iv. Indeed, Beley et al. only detected a trace amount of CO in basic pH (~ 10.6) at an applied potential of -1.05 V[37]. Our result of CO selectivity can be only

achieved in the range of 1.8 < pH < 7.31 is consistent with this experimental observation. Subsequent proton transfer to $[LNi\text{-}COOH]^+$ (step vi) results in a spontaneous C-O bond cleavage, forming water and $[LNi\text{-}CO]^{2+}$. The dissociation of $[LNi\text{-}CO]^{2+}$ into $[LNi]^{2+}$ and CO is also exergonic (step vii), indicating that the regeneration of the catalyst following CO adduct formation is spontaneous.

Pd(II) Cyclam Complex. On the Pd cyclam complex, the reduction potential of $[LPd\text{-}COO]^+$ to $[LPd\text{-}COO]^0$ is -1.00 V (step iv). This reduction potential lies in the range of typically applied potentials for CO_2 reduction (-1 ~ -1.3 V[58-60]), indicating that SEPT (step iv and v) is a likely route for $[LPd\text{-}COOH]^+$ formation. The calculated pK_a of $[LPd\text{-}COOH]^+$ is 4.37, which indicates that CPET (step iii) is not the dominant pathway in neutral pH. The proton transfer to $[LPd\text{-}COOH]^+$ causes the C-O bond cleavage, forming $[LPd\text{-}CO]^{2+}$ and water (step vi). The reaction free energy of this step indicates an exergonic reaction. CO desorption from $[LPd\text{-}CO]^{2+}$ is also exergonic, resulting in spontaneous regeneration of the catalyst (step vii).

The Hydride Cycle. Figure 6 shows the complete hydride cycle for CO_2 reduction to $HCOO^-$ and proton reduction to H_2. The hydride cycle leads through the protonation of $[LM]^{(n-1)}$ to a proton adduct ($[LM\text{-}H]^{(n)}$) (step ii). Once $[LM\text{-}H]^n$ is formed, it may subject to further one-electron reduction, resulting in the formation of complex metal hydride ($[LM\text{-}H]^{(n-1)}$) (step iii). This $[LM\text{-}H]^{(n-1)}$ can react either with CO_2 to form $HCOO^-$ or with a proton to evolve H_2, and then returns the catalyst to its initial state. The selectivity of $HCOO^-$ in the hydride cycle is determined by the reaction free energy difference between $HCOO^-$ formation ($\Delta G^{\circ}_{rxn}(HCOO^-)$) (step iva) and H_2 evolution ($\Delta G^{\circ}_{rxn}(H_2)$) (step ivb).

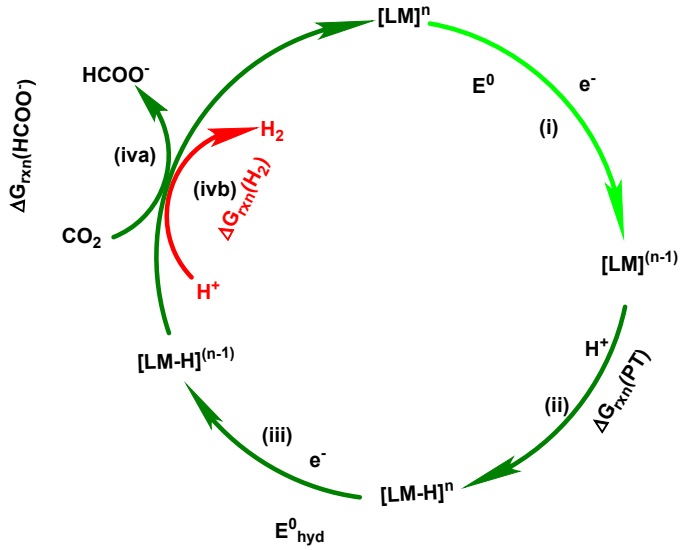

Figure 6. Hydride cycle for CO_2 reduction to $HCOO^-$ and proton to H_2. Bright green color shows shared step with CO cycle.

Most metal-cyclam complexes favor the hydride cycle energetically because pK_a of $[LM\text{-}H]^n$ with these metal ions is higher than 14. The calculated reduction potentials for the first electron transfer step (step i, E°), pK_a values of $[LM\text{-}H]^n$, the reduction potential of $[LM\text{-}H]^n$ (step iii, E°_{hyd}) and BDFEs of M-H bond in $[LM\text{-}H]^{(n-1)}$ are presented in Chart 1.

The selectivity between $HCOO^-$ and H_2 catalyzed by these metal-cyclam complexes depends on the difference between the reaction free energy of $[LM\text{-}H]^{(n-1)}$ reacting with CO_2 (step iva) and that combining with proton (step ivb). Because $HCOO^-$ is thermodynamically stable at pH higher than 7.40[51], pH = 7.40 sets the low limit for CO_2 reduction to $HCOO^-$. At pH > 7.40, HCO_3^- and CO_3^{2-} in addition to $CO_{2(g)}$ could participate in the reaction with $[LM\text{-}H]^{(n-1)}$, as shown in equations (7-9). The corresponding reaction free energies have been presented in Table S3 of Supporting Information.

$$[LM\text{-}H]^+ + CO_{2(g)} \longrightarrow [LM]^{2+} + HCOO^- \quad :\Delta G^\circ_{rxn}(HCOO)_{(CO2(g))} \quad (7)$$

$$[LM\text{-}H]^+ + HCO_3^-{}_{(aq.)} \longrightarrow [LM]^{2+} + OH^- + HCOO^- \quad :\Delta G^\circ_{rxn}(HCOO)_{(HCO3-)} \quad (8)$$

$$[LM\text{-}H]^+ + CO_3^{2-}{}_{(aq.)} + H_2O_{(l)} \longrightarrow [LM]^{2+} + 2OH^-_{(aq.)} + HCOO^- \quad :\Delta G^\circ_{rxn}(HCOO)_{(CO3--)} \quad (9)$$

The reaction free energies for $HCOO^-$ formation from $CO_{2(g)}$, HCO_3^- and CO_3^{2-} follows a trend of $\Delta G^\circ_{rxn}(HCOO^-)_{(CO2(g))} < \Delta G^\circ_{rxn}(HCOO^-)_{(HCO3-)} < \Delta G^\circ_{rxn}(HCOO^-)_{(CO3--)}$, with $\Delta G^\circ_{rxn}(HCOO^-)_{(CO2(g)),}$ being 4.37 kJ/mol lower than $\Delta G^\circ_{rxn}(HCOO^-)_{(HCO3-)}$. Therefore, $CO_{2(g)}$ is thermodynamically the most favorable reactant. On the other hand, HCO_3^- may contribute to the formation of the $HCOO^-$ species under the more basic conditions as it is the most abundant and only less favorable by 4.37 kJ/mol in reaction free energy, consistent with the experimental results[56, 61-65]. In the remaining discussion, $\Delta G^\circ_{rxn}(HCOO^-)_{(CO2(g))}$ will be used since it is the lowest among these reaction free energies.

For the competing hydrogen evolution, water or HCO_3^- (step ivb in Figure 6) can supply proton, as shown in eqn. 10 and 11,

$$[LM\text{-}H]^+ + H_2O_{(l)} \longrightarrow [LM]^{2+} + OH^-_{(aq.)} + H_{2(g)} \quad :\Delta G^\circ_{rxn}(H_2)_{(H2O)} \quad (10)$$

$$[LM\text{-}H]^+ + HCO_3^-{}_{(aq.)} \longrightarrow [LM]^{2+} + CO_3^{2-}{}_{(aq.)} + H_{2(g)} \quad :\Delta G^\circ_{rxn}(H_2)_{(HCO3-)} \quad (11)$$

The corresponding reaction free energies ($\Delta G^\circ_{rxn}(H_2)_{(H2O)}$ and $\Delta G^\circ_{rxn}(H_2)_{(HCO3-))}$) have been included in Table S3 of Supporting Information. Hydrogen evolution reaction is more favorable with HCO_3^- being the proton source than H_2O, as indicated by the reaction free energy difference of $\Delta G^\circ_{rxn}(H_2)_{(H2O)} - \Delta G^\circ_{rxn}(H_2)_{(HCO3-)} = 21.38$ kJ/mol. Since water is available throughout the entire pH range, we use $\Delta G^\circ_{rxn}(H_2)_{(H2O)}$ to compare reactions under different conditions. The difference between $\Delta G^\circ_{rxn}(HCOO^-)_{(CO2(g))}$ and $\Delta G^\circ_{rxn}(H_2)_{(H2O)}$ is constant, as shown in eqn. 12.

$$\Delta G^\circ_{rxn}(HCOO^-)_{(CO2(g))} = \Delta G^\circ_{rxn}(H_2)_{(H2O)} - 34.88 \text{ kJ/mol} \quad (12)$$

Eqn. 12 shows that $\Delta G^{\circ}_{rxn}(HCOO^-)_{(CO2(g))}$ is 34.88 kJ/mol lower than $\Delta G^{\circ}_{rxn}(H_2)_{(H2O)}$, indicating that $HCOO^-$ formation is always favored over hydrogen evolution under basic conditions where H_2O is the primary source of the proton.

$\Delta G^{\circ}_{rxn}(HCOO^-)_{CO2(g)}$ can be divided into reaction free energies of a stepwise process consisting of homolytic dissociation of the metal hydride complex followed by oxidation of $[LM]^{(n-1)}$ and simultaneous reduction of H^0 to H^- and the combination of H^- with CO_2 to form $HCOO^-$, as shown in Figure 7. Oxidation of $[LM]^{(n-1)}$ is the reverse of $[LM]^n$ reduction, and the reaction free energy equals $-nFE^{\circ}$. Since E° is negative, the reaction free energy for oxidation is positive. The reaction free energy for the reduction of H^0 to H^- is constant at -77.82 kJ/mol, and the combination of H^- with CO_2 to form $HCOO^-$ is also constant at -100.83 kJ/mol[51], which sum to -178.65 kJ/mol, as shown in eqn. 13.

$$\Delta G_{rxn}(HCOO^-)_{(CO2(g))} = \text{BDFE} - 178.65 + 96.48E^{\circ} \quad (13)$$

Chart 1. Calculated $\Delta G^{\circ}_{rxn}(HCOO^{-})_{(CO2(g))}$, shown as ΔG°_{rxn}, reduction potentials of $[LM]^{n}$ with n = 2+, 1+ and 3+ , shown as E°, pK_a values of $[LM\text{-}H]^{n}$, reduction potentials of $[LM\text{-}H]^{n}$ (E°_{hyd}) and BDFEs.

	Group 6			Group 7			Group 8		Group 9		Group 10
		$[LCr]^{2+}$	**$[LCr]^{+}$**		**$[LMn]^{2+}$**	**$[LMn]^{+}$**	**$[LFe]^{2+}$**	**$[LFe]^{+}$**	**$[LCo]^{2+}$**	**$[LCo]^{+}$**	
ΔG°_{rxn}(kJ/mol)		-121.10	-139.84		-106.19	-225.58	-111.05	-94.42	-101.50	-173.84	
E° (V)		-3.00	-3.32		-1.80	-4.27	-2.17	-3.47	-1.57	-3.34	/
E°_{hyd} (V)	/	-0.91	-3.20	/	-0.67	-3.03	-0.41	-2.00	-0.55	-2.31	
pK_a		54.26	94.15		32.45	92.34	32.64	82.75	26.26	73.60	
BDFE (kJ/mol)		347.70	359.99		245.80	365.77	277.45	410.48	228.33	327.87	
	$[LMo]^{3+}$	**$[LMo]^{2+}$**	**$[LMo]^{+}$**		**$[LTc]^{2+}$**	**$[LTc]^{+}$**	**$[LRu]^{2+}$**	**$[LRu]^{+}$**	**$[LRh]^{2+}$**	**$[LRh]^{+}$**	
ΔG°_{rxn}(kJ/mol)	125.40	-16.80	-163.53		-62.01	-126.92	24.40	-116.15	-74.48	-149.67	
E° (V)	-0.48	-1.33	-3.21	/	-1.86	-2.84	-1.05	-2.34	-0.70	-3.31	
E°_{hyd} (V)	1.41	-1.95	-2.91		-1.05	-2.53	-0.36	-2.51	-1.42	-1.49	/
pK_a	14.48	61.98	83.23		46.83	77.00	36.66	70.02	31.30	63.22	
BDFE (kJ/mol)	350.43	290.70	325.32		296.40	326.12	305.17	288.27	172.56	348.57	
	$[LW]^{3+}$	**$[LW]^{2+}$**	**$[LW]^{+}$**	**$[LRe]^{3+}$**	**$[LRe]^{2+}$**	**$[LRe]^{+}$**	**$[LOs]^{2+}$**	**$[LOs]^{+}$**	**$[LIr]^{2+}$**	**$[LIr]^{+}$**	**$[LPt]^{2+}$**
ΔG°_{rxn}(kJ/mol)	-20.67	-82.12	-120.21	83.40	25.67	-130.80	50.78	-106.70	-66.73	-149.43	-132.66
E° (V)	-1.54	-1.88	-2.77	- 0.82	-1.08	-2.84	-0.91	-2.16	-0.79	-3.34	-1.99
E°_{hyd} (V)	- 0.44	-2.17	-2.18	0.17	-1.41	-2.70	-0.58	-2.55	-1.79	-1.64	-0.24
pK_a	38.17	62.62	74.34	33.91	55.06	79.20	42.44	69.34	26.62	66.45	22.89
BDFE (kJ/mol)	306.57	278.68	335.43	341.20	308.55	322.60	317.72	281.25	188.23	351.61	238.71

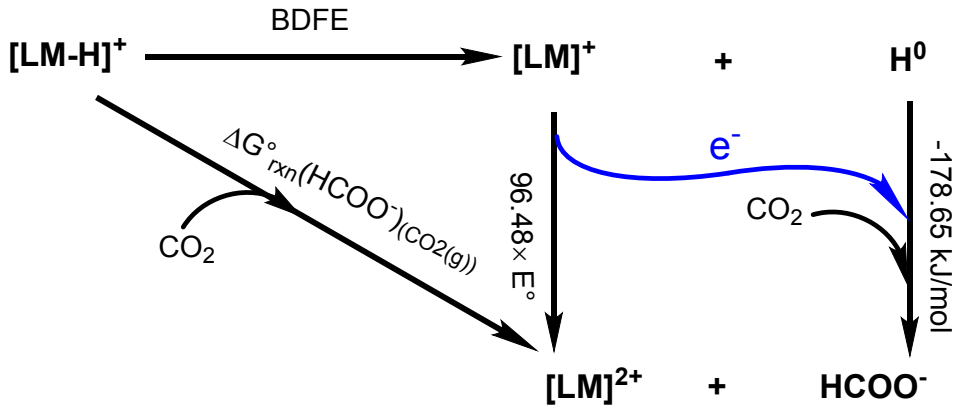

Figure 7. Correlation of BDFE of M-H bond, first reduction potential of electrocatalyst (E˚) and $\Delta G^{\circ}_{rxn}(HCOO^-)_{CO2(g)}$.

Eqn. 13 dictates a linear relationship between $\Delta G^{\circ}_{rxn}(HCOO^-)_{CO2(g)}$ and E˚, with a slope of 96.48 and intercept of -178.65. BDFEs calculated using eqn. 13 for all metal centers are presented in Chart 1. A plot of $\Delta G^{\circ}_{rxn}(HCOO^-)_{CO2(g)}/\Delta G^{\circ}_{rxn}(H_2)_{H2O}$ versus E˚ is shown in Figure 8. Based on ΔG°_{rxn} $(HCOO^-)_{CO2(g)}$ and $\Delta G^{\circ}_{rxn}(H_2)_{H2O}$, metal-cyclam complexes in Figure 8 can be roughly divided into three groups: (i) $\Delta G^{\circ}_{rxn}(HCOO^-)_{CO2(g)} > 0$, $\Delta G^{\circ}_{rxn}(H_2)_{H2O} > 0$ (white region); (ii) ΔG°_{rxn} $(HCOO^-)_{CO2(g)} < 0$, $\Delta G^{\circ}_{rxn}(H_2)_{H2O} > 0$; (green region) and (iii) $\Delta G^{\circ}_{rxn}(HCOO^-)_{CO2(g)} < 0$ and ΔG°_{rxn} $(H_2)_{H2O} < 0$ (yellow and grey regions). Group (i) includes $[LMo]^{3+}$, $[LRe]^{3+}$, $[LOs]^{2+}$, $[LRe]^{2+}$ and $[LRu]^{2+}$ (white region), group (ii) $[LMo]^{2+}$ and $[LW]^{3+}$ only (green region) and group (iii) all the rest complexes (yellow and grey regions). The cyclam complexes of group (i) will not be active for either CO_2 reduction or H_2 evolution, group (ii) will selectively reduce CO_2 to $HCOO^-$ while suppressing H_2 evolution, and group (iii) will produce both $HCOO^-$ and H_2 spontaneously. Group (iii) region is divided into grey and yellow region based on the standard reduction potential of CO_2 to $CO_2^{\bullet-}$ anion (-1.9 V). The complexes having a first reduction potential higher than -1.9 V are

not considered as catalysts. However, those complexes are included for completeness. The complexes in green and yellow regions are potential catalysts for CO_2 reduction.

The data in Figure 8 can be quantitatively regressed into two straight lines, with intercepts of 180.40 (±5.60) and 93.80 (±3.61) kJ/mol, respectively. The first line passes (blue line) through $[LMn]^+$, $[LCo]^+$, $[LCr]^+$, $[LW]^+$, $[LMo]^+$, $[LIr]^+$, $[LRh]^+$, $[LCr]^{2+}$, $[LTc]^+$, $[LRe]^+$, $[LRu]^+$, $[LOs]^+$, $[LFe]^{2+}$, $[LTc]^{2+}$, $[LW]^{3+}$ $[LMo]^{2+}$, $[LRu]^{2+}$, $[LRe]^{2+}$, $[LOs]^{2+}$, $[LRe]^{3+}$ and $[LMo]^{3+}$. The calculated BDFE using the intercept of the first line is 324.17 (± 5.60) kJ/mol. This line overlaps the $\Delta G^{\circ}_{rxn}(HCOO^-)_{CO2(g)} < 0$ and $\Delta G^{\circ}_{rxn}(H_2)_{H2O} > 0$ region in a reduction potential range of -1.4 to -1.8 V. The second line connects $[LCo]^{2+}$, $[LW]^{2+}$ $[LMn]^{2+}$ and $[LPt]^{2+}$ and has an intercept of 93.80 (±3.61) kJ/mol, resulting in a BDFE of 237.57 (±3.61) kJ/mol. The second line overlaps the $\Delta G^{\circ}_{rxn}(HCOO^-)_{CO2(g)} < 0$ and $\Delta G^{\circ}_{rxn}(H_2)_{H2O} > 0$ region in reduction potential range of -0.6 to -1.0 V. $[LFe]^+$ (left end) and $[LIr]^{2+}$and $[LRh]^{2+}$ (right end) do not fit in either of the two lines.

A low limiting potential is highly desirable for CO_2 reduction as it is critical to achieve an overall high energy efficiency. The limiting potential for CO_2 reduction to $HCOO^-$ is determined by the first reduction potential of the catalyst. Figure 8 correlates $\Delta G^{\circ}_{rxn}(HCOO^-)_{CO2(g)}$ with the first reduction potential of the catalysts. For the same metal center, the limiting potential increases as the formal oxidation number decreases and follows an order of 3+ state < 2+ state < 1+ state. Among the complexes, the limiting potential of $[LRh]^{2+}$ is the lowest and $[LIr]^{2+}$ is the close second. However, Rh and Ir are precious metals and not economical for practical applications. The next group includes $[LMo]^{2+}$, $[LW]^{2+}$, $[LCo]^{2+}$ and $[LW]^{3+}$. These metals are earth-abundant and significantly less expensive. More importantly, ($[LMo]^{2+}$ and $[LW]^{3+}$) are selective to $HCOO^-$ while suppressing hydrogen evolution, making them attractive as catalysts for electrochemical reduction of CO_2 to $HCOO^-$. These results also indicate the initial complex may need more than one electron

reduction before becoming an active center for CO_2 reduction. Two electron reduction of the metal center to activate the complex for CO_2 reduction has been reported on cobalt aminopyridine[66]. Simultaneous reduction of Ni cyclam with CO_2 was also reported[39].

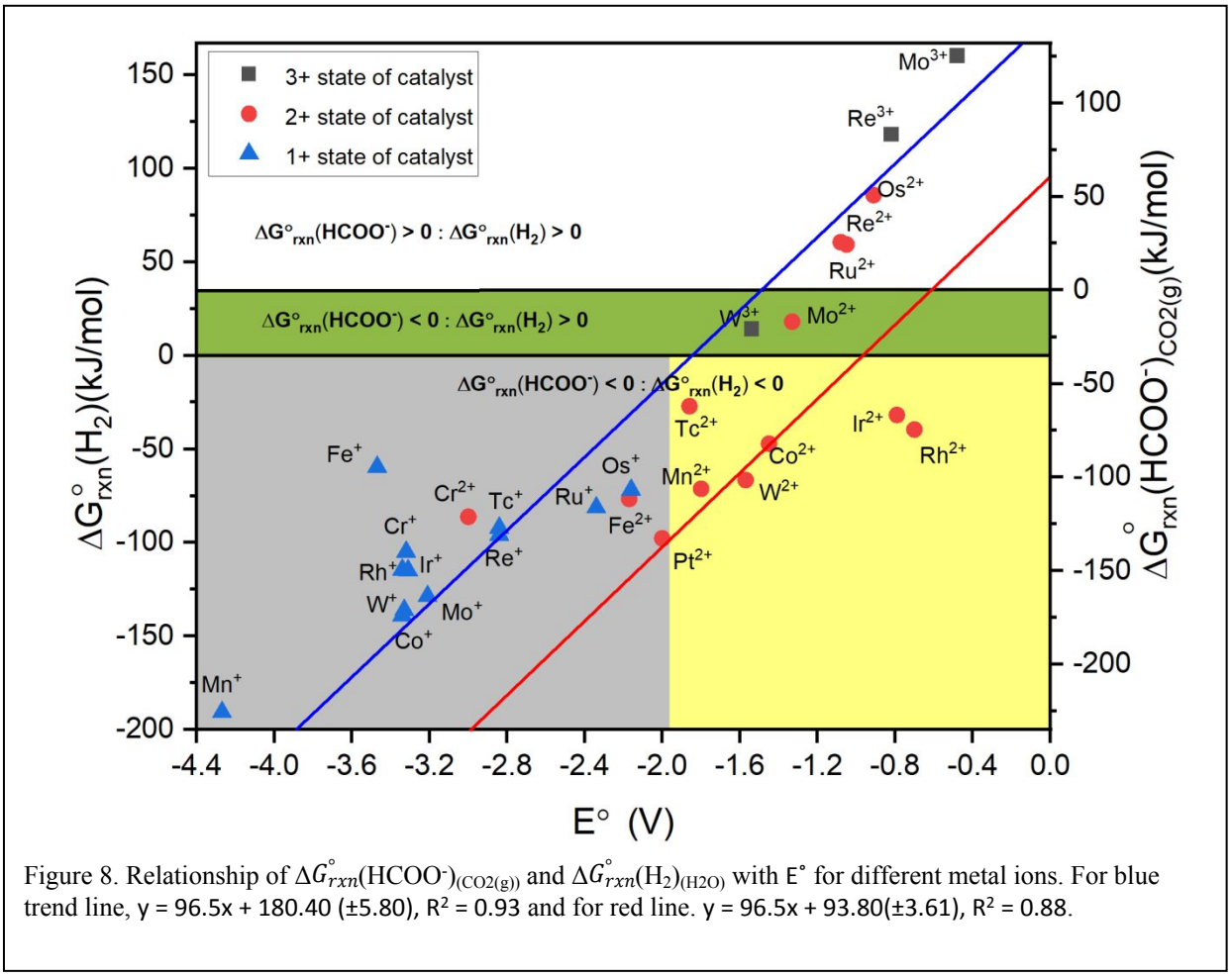

Figure 8. Relationship of $\Delta G^{\circ}_{rxn}(HCOO^-)_{(CO2(g))}$ and $\Delta G^{\circ}_{rxn}(H_2)_{(H2O)}$ with E° for different metal ions. For blue trend line, y = 96.5x + 180.40 (±5.80), R^2 = 0.93 and for red line. y = 96.5x + 93.80(±3.61), R^2 = 0.88.

We further examined the hydride transfer from $[LM\text{-}H]^{(n-1)}$ to CO_2 using constrained structural relaxation, allowing us to validate the prediction based on the correlation between $\Delta G^{\circ}_{rxn}(HCOO^-)_{CO2(g)}$ and limiting potentials. For the catalysts that catalyze $HCOO^-$ formation, i.e. $\Delta G^{\circ}_{rxn}(HCOO^-)_{CO2(g)} < 0$, H^- at the metal center of $[LM\text{-}H]^{(n-1)}$ will be transferred to CO_2, resulting in $HCOO^-$ formation. The constrained structural relaxation starts by aligning the C atom of CO_2, the

H atom and metal ion of $[LM-H]^{(n-1)}$ linearly and roughly in perpendicular to the plane formed by the N atoms of the complex, as shown in Figure 9. This initial structure was then allowed to relax along the M-H-C coordinate. We started from $[LMo-H]^+$ with CO_2 at initial distances between Mo and C of 4.5 Å, 4.0 Å and 3.5 Å and found that hydride transfer occurred for an initial distance of 3.5 Å. At 4.5 and 4.0 Å, CO_2 drifted away from the complex as the relaxation progressed. We then used 3.5 Å as the initial distance for CO_2 with $[LRh-H]^+$ and $[LCo-H]^+$ of group iii as well as $[LRe-H]^+$ of group i in the constrained structural relaxation and summarized the results in Figure 9. As shown in Figure 9, CO_2 abstracted H^- from $[LMo-H]^+$, $[LRh-H]^+$ and $[LCo-H]^+$ at an initial distance of 3.5 Å, resulting in $HCOO^-$. In contrast, there was no hydride transfer from $[LRe-H]^+$ at the same initial distance and the CO_2 molecule ended up drifting away from the complex. These results directly support the predicted reactivity of these metal-cyclam complexes for CO_2 reduction, i.e. the group ii and iii complexes enable spontaneous reduction of CO_2 to $HCOO^-$ following the hydride cycle while the group i complexes do not facilitate CO_2 reduction.

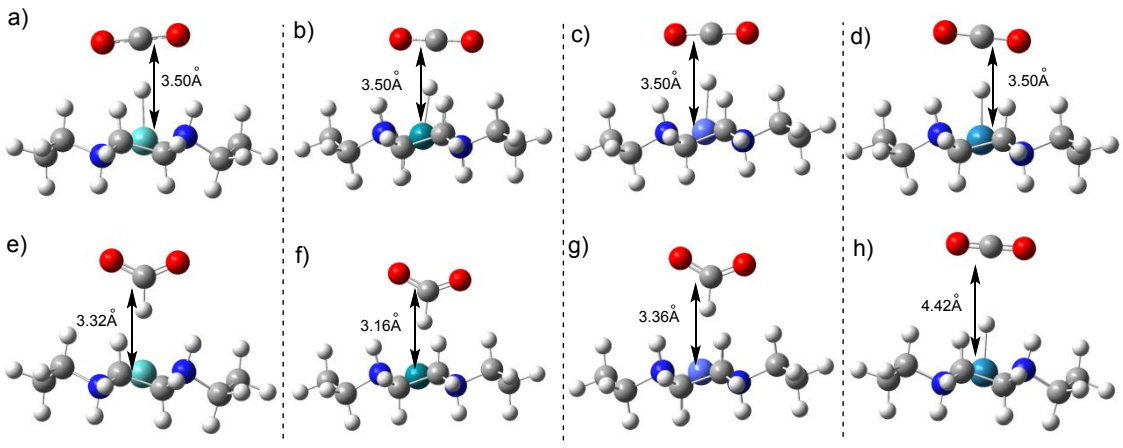

Figure 9. Initial geometries (a), (b), (c), and (d) and relaxed geometries (e),(f), (g) and (h) showing hydride transfer from the metal center to CO_2 from $[LM-H]^+$; with M = Mo (a,e) , Rh(b,f) , Co (c,g) , and Re (d,h), respectively.

We then analyzed charge partition between CO_2 and $[LM\text{-}H]^+$ before and after the hydride transfer for $[LMo\text{-}H]^+$, $[LRh\text{-}H]^+$ and $[LCo\text{-}H]^+$ and presented the results in Table S4 of Supporting Information. The results show that while the charge on the H atom of $[LM\text{-}H]^+$ in the initial configuration is not -1 (-0.62 for $[LMo\text{-}H]^+$, -0.53 for $[LRh\text{-}H]^+$ and -0.70 for $[LCo\text{-}H]^+$), the total charge on the HCOO group upon the [LM]-H-COO^- adduct formation is very close to -1 ($\geq$ -0.90), indicating a complete transfer of H^-. Following the hydride transfer to CO_2, the total charge on the cyclam complex becomes 1.94 for $[LMo]^{2+}$, 1.90 for $[LRh]^{2+}$ and 1.96 for $[LCo]^{2+}$, indicating the regeneration of the initial catalyst.

General Discussion. The results show that binding of proton and CO_2 at the reduced metal center led to the hydride and CO cycles through the $[LM\text{-}H]^n$ and $[LM\text{-}COO]^{(n-1)}$ adducts, respectively. $[LM\text{-}H]^n$ can be further reduced to metal-hydride, which may then react with CO_2 to form $HCOO^-$ or with a proton to produce hydrogen. On the other hand, $[LM\text{-}COO]^{(n-1)}$ can be reduced to CO through further protonation and reduction.

The pK_a of $[LM\text{-}H]^n$ can be treated as a descriptor to determine whether protonation of $[LM]^{(n-1)}$ is spontaneous or not. Protonation of reduced metal center enables the hydride cycle at a pH lower than the pK_a of $[LM\text{-}H]^n$ (see eqn. 4). At a pH higher than the pK_a of $[LM\text{-}H]^n$, protonation of $[LM]^{(n-1)}$ becomes endergonic, which will open up the metal center for direct CO_2 binding and steer the reaction to the CO cycle. Both kinetics and thermodynamics contribute to the observed selectivity of electrochemical CO_2 reduction and the coordination environment of the metal center could play important roles[22, 67]. Previous experimental studies showed that HER was dominant for pH < 3 whereas CO_2 reduction to CO became dominant for pH > 3 on the Co-porphyrin catalysts[68]. Similarly, hydrogen was the only product at pH = 3.7 whereas a faradic efficiency of > 90% for CO at pH = 6.7 was reported on iron porphyrin[69] .The pH-dependent selectivity reported in those

studies indicate that the kinetic barrier for protonation of the reduced metal center is low. We note that aqueous solution has been assumed for CO_2 reduction in the present study. The kinetics and thermodynamics for CO_2 reduction on a metal center with a different coordination environment in a different solvent can be very different, as shown on the Lehn-type catalysts[67, 70].

Protonation of $[LM\text{-}COO]^{(n-2)}$ in the CO cycle is also a pH-dependent reaction. The pH needs to be maintained at a value lower than the pK_a of $[LM\text{-}COOH]^{(n-1)}$ to facilitate the reduction of $[LM\text{-}COO]^{(n-2)}$ through CPET (step iii, Figure 5). We note, however, the pH has to be high enough to prevent protonation of $[LM]^{(n-1)}$. Therefore, a working pH for selective CO production can be established in the range of higher than the pK_a of $[LM\text{-}H]^n$ but lower than the pK_a of $[LM\text{-}COOH]^{(n-1)}$. For the CO-selective catalysts identified in this study, the operating pH values are in the range of 1.81 to 7.31 for $[LNi]^{2+}$ and higher than 6.10 for $[LPd]^{2+}$, respectively. The Ni-cyclam complex has already been shown as a CO selective catalyst[37, 39, 60] in medium acidic to neural pHs and we predicted that the Pd-cyclam complex is also CO-selective under more basic pHs. On the other hand, if pK_a of $[LM\text{-}COOH]^{(n-1)} \leq pK_a$ of $[LM\text{-}H]^n$, both hydride and CO cycles become accessible in an aqueous medium, resulting in mixed products. For example, both CO and hydride cycles are possible and will produce CO, $HCOO^-$ and H_2 on $[LPd]^{2+}$ with an operating pH below 4.37 (pK_a of $[LPd\text{-}COOH]^+$).

The pK_a of $[LM\text{-}H]^n$ for the majority of metal-cyclam complexes studied here is higher than 14, making protonation of $[LM]^{(n-1)}$ spontaneous even at the most basic pH level. These complexes will catalyze the reactions through the hydride cycle. The $[LM\text{-}H]^n$ can be reduced to $[LM\text{-}H]^{(n-1)}$, which will then react with CO_2 or proton to produce $HCOO^-$ or H_2. The difference between the reaction free energies for $HCOO^-$ and H_2 formation ($\Delta G^{\circ}_{rxn}(HCOO^-)_{CO2(g)} - \Delta G^{\circ}_{rxn}(H_2)_{(H2O)} = -34.88$ kJ/mol) indicates that $HCOO^-$ formation is always thermodynamically favorable and provides an

energy window that we can use to select catalysts that are $HCOO^-$ selective while suppressing hydrogen evolution. Based on this criterion, we predicted that $[LMo]^{2+}$ and $[LW]^{3+}$ are $HCOO^-$ selective catalysts. We also demonstrated that there is a correlation between $\Delta G^{\circ}_{rxn}(HCOO^-)_{CO2(g)}$ and limiting potential of catalyst. The BDFE of M-H bond in metal-hydride determines the difference in limiting potentials for catalysts with a similar $\Delta G^{\circ}_{rxn}(HCOO^-)_{CO2(g)}$, indicating that BDFE can be used as a descriptor to select a catalyst with low limiting potential. A similar linear correlation between the first reduction potential of electrocatalysts and hydricity for a small data set has been reported for the hydride of Ni bis($P^R_2N^{R'}_2$) and Pd bis(diphosphine) complexes[71-74]. Furthermore, Waldie et al. based on comprehensive thermodynamic data of 51 complexes also confirmed this correlation[26].

III. Conclusions

Electrochemical CO_2 reduction to CO and $HCOO^-$ on the metal-cyclam complex molecular catalysts with group 6-10 transition metal ions have been studied using the DFT computational method. Our results show that the pH relative to the pK_a of $[LM\text{-}H]^n$ determines whether $[LM]^{(n-1)}$ can be protonated to steer the reaction to the hydride. On the other hand, the pK_a of $[LM\text{-}COOH]^{(n-1)}$ determines the upper bound of pH for the protonation of the CO_2 adduct. Our results show that $[LNi]^{2+}$ and $[LPd]^{2+}$ are selective to CO in pH ranges of 1.81 to 7.31 and 6.10 and higher, respectively. This conclusion of $[LNi]^{2+}$ being CO selective in acidic pH is consistent with the experimental results.

The formation free energy of $HCOO^-$ from $CO_{2(g)}$ was used to select a metal-cyclam complex as a catalyst for electrochemical CO_2 reduction following the hydride cycle. Based on the formation free energy difference between $HCOO^-$ and hydrogen, $[LMo]^{2+}$ and $[LW]^{3+}$ were

predicted to be selective to $HCOO^-$ while suppressing hydrogen formation. Other catalysts, including $[LRh]^{2+}$, $[LIr]^{2+}$, $[LW]^{2+}$, $[LCo]^{2+}$ and $[LTc]^{2+}$ can reduce CO_2 to $HCOO^-$ while produce hydrogen simultaneously. Among them, $[LRh]^{2+}$ has the lowest limiting potential and $[LIr]^{2+}$ is the close second. The limiting potentials for $[LMo]^{2+}$, $[LW]^{3+}$ and $[LCo]^{2+}$ are in -1.6 to -1.3 V, making them promising catalysts for electrochemical reduction of CO_2. Since Co, Mo and W are earth-abundant, the catalysts based on them are more attractive for practical application. The present study will likely stimulate further interests in experimentally exploring the metal-cyclam complexes as CO_2 reduction catalysts and the approach will be applicable to screen and select other metal complexes as efficient and selective CO_2 reduction catalysts.

IV. Computational Details

All DFT calculations were carried out using Gaussian 16[75] with the B3LYP hybrid functional[76]. Grimme's D3 dispersion corrections were applied in all calculations[77]. The Stuttgart-Dresden effective core potential[78] for transition metal elements and 6-31g(d,p) basis set for the main group elements were used for geometry optimization and frequency analysis. The type-4 continuum solvation model (SMD) was used to represent water as an implicit solvent[79]. The stability of wavefunctions for all species has been checked. The spin multiplicity of the resulting ground states of individual complexes has been listed in Tables S5(a) and (b) of Supporting Information.

The pK_a values of protonated species and reduction potentials of electron transfer steps were calculated based on the corresponding reaction free energy. The reduction potentials were reported by using the standard hydrogen electrode (SHE) as the reference. The detailed procedures for determining pK_a and reduction potentials have been provided in Section S1 and S2 of the Supporting Information. Thermodynamic cycles used to determine the free energy (G°) of the

reactive anions, including OH^-, $HCOO^-$, HCO_3^- and CO_3^{2-}, have been detailed in Section S3 of the Supporting Information. Bader's atom in molecule (AIM) charge[80] analysis was performed using Multiwfn program[81].

Conflicts of interest

The authors declare no competing financial interest.

Acknowledgments

This work was supported by the National Science Foundation (NSF-CBET, No.1438440).

References

1. A. M. Appel, J. E. Bercaw, A. B. Bocarsly, H. Dobbek, D. L. DuBois, M. Dupuis, J. G. Ferry, E. Fujita, R. Hille and P. J. Kenis, *Chem. Rev.*, 2013, **113**, 6621-6658.
2. G. n. O. Larrazábal, A. J. Martín and J. Perez-Ramirez, *J. Phys. Chem. Lett.*, 2017, **8**, 3933-3944.
3. C. Costentin, M. Robert and J.-M. Savéant, *Chem. Soc. Rev.*, 2013, **42**, 2423-2436.
4. S. Das, J. Pérez-Ramírez, J. Gong, N. Dewangan, K. Hidajat, B. C. Gates and S. Kawi, *Chem. Soc. Rev.*, 2020, **49**, 2937-3004.
5. G. Wang, J. Chen, Y. Ding, P. Cai, L. Yi, Y. Li, C. Tu, Y. Hou, Z. Wen and L. Dai, *Chem. Soc. Rev.*, 2021, DOI: 10.1039/D0CS00071J.
6. N. Elgrishi, M. B. Chambers, X. Wang and M. Fontecave, *Chem. Soc. Rev.*, 2017, **46**, 761-796.
7. E. Boutin, L. Merakeb, B. Ma, B. Boudy, M. Wang, J. Bonin, E. Anxolabéhère-Mallart and M. Robert, *Chem. Soc. Rev.*, 2020, **49**, 5772-5809.
8. Y. Y. Birdja, J. Shen and M. T. Koper, *Catal. Today*, 2017, **288**, 37-47.
9. H. Takeda, C. Cometto, O. Ishitani and M. Robert, *ACS catal.*, 2017, **7**, 70-88.
10. P. Sen, B. Mondal, D. Saha, A. Rana and A. Dey, *Dalton Trans.*, 2019, **48**, 5965-5977.
11. P. Gotico, Z. Halime and A. Aukauloo, *Dalton Trans.*, 2020, **49**, 2381-2396.
12. S. Amanullah, P. Saha, A. Nayek, M. E. Ahmed and A. Dey, *Chem. Soc. Rev.*, 2021, **50**, 3755-3823.
13. G. F. Manbeck and E. Fujita, *J. Porphyrins Phthalocyanines*, 2015, **19**, 45-64.
14. A. J. Göttle and M. T. Koper, *J. Am. Chem. Soc.*, 2018, **140**, 4826-4834.
15. J. Shen, M. J. Kolb, A. J. Gottle and M. T. Koper, *J. Phys. Chem. C*, 2016, **120**, 15714-15721.
16. M. Abdinejad, C. Dao, B. Deng, F. Dinic, O. Voznyy, X.-a. Zhang and H.-B. Kraatz, *ACS Sustain. Chem. Eng.*, 2020, **8**, 9549-9557.
17. N. Furuya and K. Matsui, *J. Electroanal. Chem. Interf. Electrochem.*, 1989, **271**, 181-191.
18. J.-H. Liu, L.-M. Yang and E. Ganz, *ACS Sustain. Chem. Eng.*, 2018, **6**, 15494-15502.
19. K. M. Waldie, F. M. Brunner and C. P. Kubiak, *ACS Sustain. Chem. Eng.*, 2018, **6**, 6841-6848.
20. P. Kang, C. Cheng, Z. Chen, C. K. Schauer, T. J. Meyer and M. Brookhart, *J. Am. Chem. Soc.*, 2012, **134**, 5500-5503.

21. B. M. Ceballos and J. Y. Yang, *Proc. Natl. Acad. Sci.*, 2018, **115**, 12686-12691.
22. B. M. Ceballos and J. Y. Yang, *Organometallics*, 2020, **39**, 1491-1496.
23. A. Taheri and L. A. Berben, *Inorg. Chem.*, 2015, **55**, 378-385.
24. N. D. Loewen, T. V. Neelakantan and L. A. Berben, *Acc. Chem. Res.*, 2017, **50**, 2362-2370.
25. S. J. Connelly Robinson, C. M. Zall, D. L. Miller, J. C. Linehan and A. M. Appel, *Dalton Trans.*, 2016, **45**, 10017-10023.
26. K. M. Waldie, A. L. Ostericher, M. H. Reineke, A. F. Sasayama and C. P. Kubiak, *ACS catal.*, 2018, **8**, 1313-1324.
27. Z.-J. Zhao, S. Liu, S. Zha, D. Cheng, F. Studt, G. Henkelman and J. Gong, *Nat. Rev. Mater.*, 2019, **4**, 792-804.
28. J. Greeley, *Annu. Rev. Chem. Biomol. Eng.*, 2016, **7**, 605-635.
29. A. A. Peterson and J. K. Nørskov, *J. Phys. Chem. Lett.*, 2012, **3**, 251-258.
30. X. Liu, J. Xiao, H. Peng, X. Hong, K. Chan and J. K. Nørskov, *Nat. Commun.*, 2017, **8**, 1-7.
31. A. Marjolin and J. A. Keith, *ACS catal.*, 2015, **5**, 1123-1130.
32. A. J. Göttle and M. T. Koper, *Chem. Sci*, 2017, **8**, 458-465.
33. J. Song, E. L. Klein, F. Neese and S. Ye, *Inorg. Chem.*, 2014, **53**, 7500-7507.
34. X. Liang and P. J. Sadler, *Chem. Soc. Rev.*, 2004, **33**, 246-266.
35. W. Nam, R. Ho and J. S. Valentine, *J. Am. Chem. Soc.*, 1991, **113**, 7052-7054.
36. E. Bounsall and S. Koprich, *Can. J. Chem.*, 1970, **48**, 1481-1491.
37. M. Beley, J.-P. Collin, R. Ruppert and J.-P. Sauvage, *J. Chem. Soc., Chem. Commun.*, 1984, 1315-1316.
38. M. Beley, J. P. Collin, R. Ruppert and J. P. Sauvage, *J. Am. Chem. Soc.*, 1986, **108**, 7461-7467.
39. J. D. Froehlich and C. P. Kubiak, *Inorg. Chem.*, 2012, **51**, 3932-3934.
40. A. Zhanaidarova, C. E. Moore, M. Gembicky and C. P. Kubiak, *Chem. Commun.*, 2018, **54**, 4116-4119.
41. M. Beley, J.-P. Collin, R. Ruppert and J.-P. Sauvage, *J. Chem. Soc., Chem. Commun.*, 1984, DOI: 10.1039/C39840001315, 1315-1316.
42. L. Roy, B. Mondal and S. Ye, *Dalton Trans.*, 2020, **49**, 16608-16616.
43. P. J. Connolly and E. J. Billo, *Inorg. Chem.*, 1987, **26**, 3224-3226.
44. H. S. Yu, X. He, S. L. Li and D. G. Truhlar, *Chem. Sci*, 2016, **7**, 5032-5051.
45. C. Kavaklı, S. A. Tuncel and B. Salih, *Sep. Purif. Technol.*, 2005, **45**, 32-40.
46. P. U. Thakker, R. G. Aru, C. Sun, W. T. Pennington, A. M. Siegfried, E. C. Marder and P. S. Wagenknecht, *Inorg. Chim. Acta*, 2014, **411**, 158-164.
47. D. Guldi, F. Wasgestian, E. Zeigerson and D. Meyerstein, *Inorg. Chim. Acta*, 1991, **182**, 131-133.
48. M. A. DeLeo and P. C. Ford, *Coord. Chem. Rev.*, 2000, **208**, 47-59.
49. B. Kumar, M. Llorente, J. Froehlich, T. Dang, A. Sathrum and C. P. Kubiak, *Annu. Rev. Phys. Chem.*, 2012, **63**, 541-569.
50. D. R. Lide, *CRC handbook of chemistry and physics*, CRC press, 2004.
51. S. J. Connelly, E. S. Wiedner and A. M. Appel, *Dalton Trans.*, 2015, **44**, 5933-5938.
52. C. Costentin and J.-M. Savéant, *Nat. Rev. Chem.*, 2017, **1**, 0087.
53. C. Costentin and J.-M. Savéant, *J. Am. Chem. Soc.*, 2018, **140**, 16669-16675.
54. C. Costentin and J.-M. Savéant, *J. Am. Chem. Soc.*, 2017, **139**, 8245-8250.
55. J. M. Barlow and J. Y. Yang, *ACS Cent. Sci.*, 2019, **5**, 580-588.
56. C. A. Kelly, Q. G. Mulazzani, M. Venturi, E. L. Blinn and M. A. Rodgers, *J. Am. Chem. Soc.*, 1995, **117**, 4911-4919.
57. J. Calabrese, T. Herskovitz and J. Kinney, *J. Am. Chem. Soc.*, 1983, **105**, 5914-5915.
58. G. B. Balazs and F. C. Anson, *J. Electroanal. Chem.*, 1992, **322**, 325-345.

59. Y. Wu, B. Rudshteyn, A. Zhanaidarova, J. D. Froehlich, W. Ding, C. P. Kubiak and V. S. Batista, *ACS catal.*, 2017, **7**, 5282-5288.
60. S. L. Behnke, A. C. Manesis and H. S. Shafaat, *Dalton Trans.*, 2018, **47**, 15206-15216.
61. K. Asada, in *Organic and bio-organic chemistry of carbon dioxide*, Tokyo: Kodansha, 1982, pp. 185-274.
62. M. Dunwell, Q. Lu, J. M. Heyes, J. Rosen, J. G. Chen, Y. Yan, F. Jiao and B. Xu, *J. Am. Chem. Soc.*, 2017, **139**, 3774-3783.
63. S. Zhu, B. Jiang, W.-B. Cai and M. Shao, *J. Am. Chem. Soc.*, 2017, **139**, 15664-15667.
64. R. Kortlever, K. H. Tan, Y. Kwon and M. T. M. Koper, *J. Solid State Electrochem.*, 2013, **17**, 1843-1849.
65. F. Bienen, D. Kopljar, A. Löwe, S. Geiger, N. Wagner, E. Klemm and K. A. Friedrich, *ACS Sustain. Chem. Eng.*, 2020, **8**, 13759-13768.
66. A. Chapovetsky, T. H. Do, R. Haiges, M. K. Takase and S. C. Marinescu, *J. Am. Chem. Soc.*, 2016, **138**, 5765-5768.
67. C. Riplinger, M. D. Sampson, A. M. Ritzmann, C. P. Kubiak and E. A. Carter, *J. Am. Chem. Soc.*, 2014, **136**, 16285-16298.
68. J. Shen, R. Kortlever, R. Kas, Y. Y. Birdja, O. Diaz-Morales, Y. Kwon, I. Ledezma-Yanez, K. J. P. Schouten, G. Mul and M. T. Koper, *Nat. Commun.*, 2015, **6**, 8177.
69. C. Costentin, M. Robert, J.-M. Savéant and A. Tatin, *Proc. Natl. Acad. Sci.*, 2015, **112**, 6882-6886.
70. J. A. Keith, K. A. Grice, C. P. Kubiak and E. A. Carter, *J. Am. Chem. Soc.*, 2013, **135**, 15823-15829.
71. B. R. Galan, J. Schöffel, J. C. Linehan, C. Seu, A. M. Appel, J. A. S. Roberts, M. L. Helm, U. J. Kilgore, J. Y. Yang, D. L. DuBois and C. P. Kubiak, *J. Am. Chem. Soc.*, 2011, **133**, 12767-12779.
72. D. E. Berning, A. Miedaner, C. J. Curtis, B. C. Noll, M. C. Rakowski DuBois and D. L. DuBois, *Organometallics*, 2001, **20**, 1832-1839.
73. U. J. Kilgore, M. P. Stewart, M. L. Helm, W. G. Dougherty, W. S. Kassel, M. R. DuBois, D. L. DuBois and R. M. Bullock, *Inorg. Chem.*, 2011, **50**, 10908-10918.
74. J. W. Raebiger, A. Miedaner, C. J. Curtis, S. M. Miller, O. P. Anderson and D. L. DuBois, *J. Am. Chem. Soc.*, 2004, **126**, 5502-5514.
75. M. Frisch, G. Trucks, H. Schlegel, G. Scuseria, M. Robb, J. Cheeseman, G. Scalmani, V. Barone, G. Petersson and H. Nakatsuji, *Gaussian Inc. Wallingford CT*, 2016, **1**.
76. P. J. Stephens, F. Devlin, C. Chabalowski and M. J. Frisch, *J. Phys. Chem.*, 1994, **98**, 11623-11627.
77. S. Grimme, J. Antony, S. Ehrlich and H. Krieg, *J. Chem. Phys.*, 2010, **132**, 154104.
78. M. Dolg, U. Wedig, H. Stoll and H. Preuss, *J. Chem. Phys.*, 1987, **86**, 866-872.
79. A. V. Marenich, C. J. Cramer and D. G. Truhlar, *J. Phys. Chem. B.*, 2009, **113**, 6378-6396.
80. W. Orville-Thomas, *Atoms in molecules—a quantum theory: Richard FW Bader, Clarendon press, Oxford, UK 1994, 438 pp.*, Elsevier, 1996.
81. T. Lu and F. Chen, *J. Comput. Chem.*, 2012, **33**, 580-592.